Multiple Conformations of an Intercalated (−)-(7*S*,8*R*,9*S*,10*R*)-N^6-[10-(7,8,9,10-Tetrahydrobenzo[a]pyrenyl)]-2′-deoxyadenosyl Adduct in the *N-ras* Codon 61 Sequence†

Irene S. Zegar,‡,§ Parvathi Chary,|| Ritche J. Jabil,|| Pamela J. Tamura,§ Tommy N. Johansen,§,⊥ R. Stephen Lloyd,|| Constance M. Harris,§ Thomas M. Harris,§ and Michael P. Stone*,§

Department of Chemistry, and Center in Molecular Toxicology, Vanderbilt University, Nashville, Tennessee 37235, and Department of Human Biological Chemistry and Genetics and Sealy Center for Molecular Science, The University of Texas Medical Branch, Galveston, Texas 77555

Received July 21, 1998; Revised Manuscript Received September 17, 1998

ABSTRACT: The structure of the (−)-(7*S*,8*R*,9*S*,10*R*)-N^6-[10-(7,8,9,10-tetrahydrobenzo[a]pyrenyl)]-2′-deoxyadenosyl adduct at A^7 of 5′-d(CGGACAAGAAG)-3′•5′-d(CTTCTTGTCCG)-3′, derived from trans addition of the exocyclic N^6-amino group of dA to (−)-(7*S*,8*R*,9*R*,10*S*)-7,8-dihydroxy-9,10-epoxy-7,8,9,10-tetrahydrobenzo[a]pyrene [(−)-DE2], was determined using molecular dynamics simulations restrained by 532 NOEs from ^{1}H NMR. This was named the SRSR(61,3) adduct, derived from the *N-ras* protooncogene at and adjacent to the nucleotides encoding amino acid 61 (underlined) of the p21 gene product. The solution structure of this adduct was best described as a mixture of two conformations in rapid equilibrium on the NMR time scale. The two populations differed in the pseudorotation angle of the sugar ring for the 5′-neighboring base A^6, as determined from scalar coupling data. One population, estimated to be present at 53%, had the A^6 deoxyribose in the C2′-endo conformation, while in the second conformation the A^6 deoxyribose was in the C3′-endo conformation. NOEs between C^5, A^6, and ^{SRSR}A^7 were either disrupted or weakened, as were those in the complementary strand between C^{15}, T^{16}, and T^{17}. Major groove NOEs were observed between the benzo[a]pyrene aromatic protons, H1, H2, H3, H4, H5, and H6, and T^{16} CH_3. Minor groove NOEs were observed between H1, H2, and H3 of benzo[a]pyrene and T^{16} H1′ and H2′ and T^{17} H1′ and H2′. The benzo[a]pyrene protons H10, H11, and H12 showed NOEs to A^6 H1′, H2′, and H2″. The chemical shifts of the pyrenyl moiety were dispersed over a 1.9 ppm range. Upfield chemical shifts of 2.4 ppm for T^{16} N3H, 1.1 ppm for T^{17} N3H, 1.3 and 1.0 ppm for T^{16} H6 and CH_3, 0.85 ppm for T^{16} H1′, and 0.80 and 0.90 ppm for C^{15} H2′ and H2″ were observed. These observations were consistent with intercalation of the pyrenyl moiety toward the 5′ direction of ^{SRSR}A^7. The results were compared to the isomeric SRSR(61,2) adduct [I. S. Zegar, S. J. Kim, T. N. Johansen, P. J. Horton, C. M. Harris, T. M. Harris, and M. P. Stone (1996) *Biochemistry 35*, 6212−6224] and revealed the role of DNA sequence in modulating the conformation of this benzo[a]pyrene adduct.

Interest in the polycyclic aromatic hydrocarbon (PAH[1]) class of chemical carcinogens dates to Percival Pott's linkage between the incidence of scrotal cancer in chimney sweeps and occupational exposure to soot. Microsomal P_{450} enzymes (*1*) catalyze the formation of diastereomeric benzo[a]pyrene 7,8-dihydrodiol-9,10-epoxides (*2*), first synthesized by the Jerina (*3*) and the Harvey (*4*) laboratories. The bay-region epoxides include (+)-(7*R*,8*S*,9*S*,10*R*)-7,8-dihydroxy-9,10-epoxy-7,8,9,10-tetrahydrobenzo[a]pyrene [(+)-DE2] and (−)-(7*S*,8*R*,9*R*,10*S*)-7,8-dihydroxy-9,10-epoxy-7,8,9,10-tetrahydrobenzo[a]pyrene [(−)-DE2].[2] Evidence that (+)-DE2 had the greatest bonding affinity to DNA was obtained from

† This research was supported by the NIH, ES-05355. Funding for the NMR spectrometer was supplied by a grant from the NIH shared instrumentation program, RR-05805, and the Vanderbilt Center in Molecular Toxicology, ES-00267. This research was also supported by the Vanderbilt Cancer Center, CA-68485. This study made use of the National Magnetic Resonance Facility at Madison. NMRFAM equipment was purchased with funds from the University of Wisconsin, NSF Grants DMB-8415048 and BIR-9214394, NIH Grants RR-02301, RR-02781, and RR-08438, and the USDA.

* To whom correspondence should be addressed. Tel: (615) 322-2589. Fax: (615) 343-1234. E-mail: stone@toxicology.mc.vanderbilt.edu.

‡ Current Address: Department of Chemistry, Pittsburg State University, Pittsburg, KS 66762.

§ Vanderbilt University.

|| The University of Texas Medical Branch.

⊥ Current Address: Department of Medicinal Chemistry, The Royal Danish School of Pharmacy, Universitetsparken 2, DK-2100 Copenhagen, Denmark.

[1] Abbreviations: BPDE, benzo[a]pyrene diol epoxide; DSS, sodium 4,4-dimethyl-4-silapentanesulfonate; EDTA, ethylenediaminetetraacetic acid; NOE, nuclear Overhauser enhancement; NOESY, two-dimensional NOE spectroscopy; ppm, parts per million; TPPI, time proportional phase increment; TOCSY, total homonuclear correlated spectroscopy; 1D, one-dimensional; 2D, two-dimensional; PAH, polycyclic aromatic hydrocarbon.

[2] The empirical designations for these diol epoxides are the (±)-*anti*-BPDE, or (±)-DE2. Benzo[a]pyrene is also metabolized into two additional diol epoxides, (+)-(7*S*,8*R*,9*S*,10*R*)-7,8-dihydroxy-9,10-epoxy-7,8,9,10-tetrahydrobenzo[a]pyrene and (−)-(7*R*,8*S*,9*R*,10*S*)-7,8-dihydroxy-9,10-epoxy-7,8,9,10-tetrahydrobenzo[a]pyrene. These are the (±)-*cis*-BPDE, or (±)-DE1, which are generally regarded to be less mutagenic and tumorigenic.

10.1021/bi9817616 CCC: $15.00
Published on Web 11/05/1998

reactions using diastereomeric mixtures of the epoxides with DNA, followed by enzymatic degradation and analysis (*5, 6*). Identification of the DNA adducts (*7, 8*) revealed an adduct formed between the 2-amino group of guanine and C10 of the PAH, with that derived from (+)-DE2 being the major product. The (+)-DE2 is generally regarded as the most mutagenic stereoisomer of the epoxide (*9, 10*). Accordingly, there has been considerable interest in the conformations of benzo[a]pyrene (*11*−*17*), related PAH (*18*), and styrene oxide (*19, 20*) adducts at guanine N^2.

Minor products in the reaction of various diastereomeric BPDE with DNA include adenine N^6 adducts (*21, 22*). These are of interest because the relation between the major and minor sites of covalent adduction and mutagenesis remains incompletely understood. Experiments using Chinese hamster V-79 cells randomly modified with (+)-DE2 revealed mutations at adenine at physiologically relevant levels of exposure (*23*−*25*). Predominantly A → C mutations occurred at low doses, with low frequencies of A → G mutations. Cells modified with (−)-DE2 yielded fewer mutations and showed less selectivity in their mutagenic profile, suggesting a role for stereochemistry in modulating the mutagenic spectra of these adducts (*24*). A series of polymerase extension studies in vitro (*26, 27*) also revealed the influence of stereochemistry upon replication.

The conformations of several adenyl N^6 benzo[a]pyrene (*28*−*32*) and benzo[*c*]phenanthrene (*33, 34*) adducts have been examined. These studies led to the recognition of the importance of adduct stereochemistry at C10 as the crucial determinant of 5′ versus 3′ intercalation of the pyrenyl moiety for adenine N^6 PAH adducts (*28*). All C10*R* isomers examined to date intercalated toward the 5′ direction, whereas the C10*S* isomers intercalated toward the 3′ direction of the modified strand (*28*−*34*).

Appreciation has also been gained for the role of DNA sequence in determining differences in adduct mutagenic potential. For benzo[a]pyrene, experiments in which double-stranded adducted vectors were replicated in *Escherichia coli* revealed that the (+)-DE2 adduct at guanine N^2 induced mostly G → T transversions in the sequence 5′-TGC-3′ (*35*) and mostly G → A mutations in the 5′-CGT-3′ sequence (*36*), while in the 5′-CGG-3′ sequence, G → T, A, and C mutations were observed (*37*). Site-specific mutagenesis experiments in which four stereoisomeric adenyl N^6 BPDE adducts were inserted into single-stranded vectors and expressed in *Escherichia coli* SMH77 revealed that both the mutation spectra and frequencies differed in the 5′-TAG-3′ sequence as compared to the 5′-GAT-3′ sequence (*38*).

These results emphasize the need to understand how DNA sequence modulates adduct conformation. Previous NMR (*39*) and fluorescence (*40*) studies have shown that at guanine N^2, flanking base effects alter the conformation of minor groove 10*S*-[BP] adducts. It was proposed that the flanking pair on the 5′ side modulated the properties of the 10*S*-[BP] minor groove adducts (*39, 41*). Our laboratory has focused on adduct conformation within crucial coding regions of the human *N-ras* protooncogene. Mutations within a limited number of codons of the p21 protein, including codons 12 and 61, cause oncogene activation (*42*). We have used the *ras61* oligodeoxynucleotide d(CGGACAAGAAG)-3′•5′-d(CTTCTTGTCCG)-3′ as a model (*43*) (Scheme 1). Studies of DNA sequence effects upon the structures of the *R*- and *S*-α-styrene oxide adducts, located either at adenine N^6 at two sites in the *ras61* oligodeoxynucleotide (*44*−*46*) or at guanine N^2 at two sites in the *ras12* oligodeoxynucleotide (*19, 20*), were performed. Both large and small sequence effects were observed for the major groove styrene adducts in the *ras61* sequence (*44*−*46*). For minor groove *ras12* adducts (*19, 20*), smaller sequence effects were observed.

Scheme 1: The SRSR(61,3) Oligodeoxynucleotide, Where X = (−)-(7*S*,8*R*,9*S*,10*R*)-N^6-[10-(7,8,9,10-Tetrahydrobenzo-[a]pyrenyl)]-2′-deoxyadenosyl Adduct (Bottom)

ras codons

60 61 62

5′-C^1 |G^2 G^3 A^4 |C^5 A^6 X^7 |G^8 A^9 A^{10}|G^{11}-3′

3′-G^{22}|$C^{21}C^{20}T^{19}$|$G^{18}T^{17}T^{16}$|$C^{15}T^{14}T^{13}$|C^{12}-5′

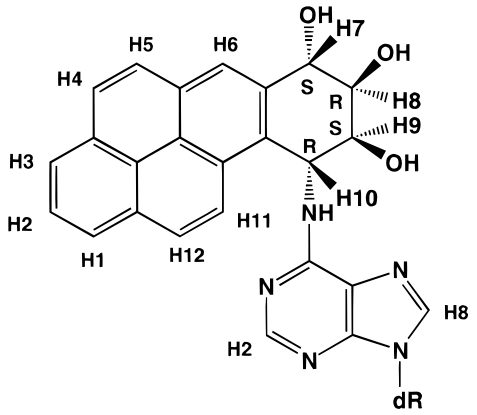

The (-) (7*S*,8*R*,9*S*,10*R*)-N6-[10-(7,8,9-trihydroxy-7,8,9,10-tetrahydrobenzo[a]pyrenyl)]-2'-deoxyadenosyl adduct and designations of the benzo[a]pyrene protons

The results of the present work provide the first view of DNA sequence effects for adenyl N^6 benzo[a]pyrene adducts located in the *ras61* oligodeoxynucleotide. This work extends a previous study which revealed that the benzo[a]-pyrenyl moiety of the SRSR(61,2)[3] adduct intercalated above the 5′ face of the modified adenine (*32*). Molecular dynamics calculations using simulated annealing and restrained by ^{1}H nuclear Overhauser effects (*47*) demonstrate that the pyrenyl moiety of the SRSR(61,3) adduct (Scheme 1) also intercalates above the 5′ face of the modified adenine. However, in contrast to the SRSR(61,2) adduct (*32*), the SRSR(61,3) adduct is best described as a mixture of two conformations in rapid equilibrium on the NMR time scale. The two populations differ in the pseudorotation angle of the sugar ring for the 5′ neighboring base A^6. The major population, estimated to be present at approximately 53%, has the A^6 deoxyribose in the C3′-endo conformation, while in the other population, the A^6 deoxyribose is in the C2′-endo conformation. This reveals the role of DNA sequence in modulating the conformation of this benzo[a]pyrene adduct, which may be important in understanding the biological processing of these lesions.

[3] This was named the SRSR(61,3) adduct, which designates the stereochemistry at C7, C8, C9, and C10 of benzo[a]pyrene, the modified codon in the *N-ras* protooncogene, and the position of the adducted adenine in this codon.

MATERIALS AND METHODS

Materials. The oligodeoxynucleotide 5′-d(CTTCTTGTC-CG)-3′ was purchased from the Midland Certified Reagent Company (Midland, TX). The modified oligodeoxynucleotide 5′-d(CGGACA^{SRSR}AGAAG)-3′ (Scheme 1) was synthesized through a nonbiomimetic procedure in which the (±)-amino triol derived from (±)-7β,8α-dihydroxy-9α,10α-epoxy-7,8,9,10-tetrahydrobenzo[a]pyrene [(±)-DE2] was reacted with an oligodeoxynucleotide containing 6-fluoroadenosine at position A[7] (*48*−*50*). The modified oligodeoxynucleotide was purified by HPLC using a reverse-phase semipreparative column (PRP-1; Hamilton Company, Reno, NV) equilibrated with 10 mM ethylenediamine acetate (pH 7.0). The oligodeoxynucleotide was eluted using a gradient consisting of 0%−20% acetonitrile in 20 min. The DNA was lyophilized and desalted on Sephadex G-25 (Pharmacia-P. L. Biochemicals, Inc., Piscataway, NJ).

NMR Samples. The concentration of 5′-d(CTTCTTGTC-CG)-3′ was determined from the calculated extinction coefficient, 1.09×10^5 (*51*). The concentration of 5′-d(CGGACA^{SRSR}AGAAG)-3′ was determined from the extinction coefficient of 2.90×10^4 M^{-1} cm^{-1} at 353 nm (*52*). The complementary oligodeoxynucleotides were mixed in equal molar proportions in 10 mM NaH_2PO_4, 0.1 M NaCl, and 50 μM Na_2EDTA, at pH 6.9. The mixture was heated to 85 °C for 5 min followed by cooling to room temperature to anneal the strands. DNA Grade Bio-Gel hydroxylapatite (Bio-Rad Laboratories, Richmond, CA) (15 cm × 3.0 cm), eluted with a gradient from 10 to 200 mM NaH_2PO_4 (pH 6.9), was used for the separation of double- from single-stranded oligodeoxynucleotides. The duplex was lyophilized, resuspended in 1 mL of H_2O, and desalted on Sephadex G-25 (70 × 1.5 cm). The sample was lyophilized and dissolved in 0.5 mL of NMR buffer [0.1 M NaCl, 5×10^{-5} Na_2EDTA, 0.01 M NaH_2PO_4 (pH 6.9)]. The final strand concentration was determined to be 1.8 mM. Strand stoichiometry was assayed by HPLC.

NMR. Spectra were recorded at 750.13 and 500.13 MHz. The sample used for observation of the nonexchangeable protons was exchanged three times in 99.96% D_2O and suspended in 0.5 mL of NMR buffer containing 99.996% D_2O, while that used for the observation of exchangeable protons was dissolved in 0.5 mL of NMR buffer containing 9:1 H_2O-D_2O. Spectra were referenced to the water resonance at 4.76 ppm at 20 °C or 4.97 ppm at 10 °C. Phase-sensitive NOESY spectra used for resonance assignments were recorded using TPPI for quadrature detection. A mixing time of 400 ms was used. In the t1 dimension, 1024 real data points were collected, with 32 acquisitions per FID with a 1.5 s relaxation delay; 2048 real data points were used in the t2 dimension. The residual water resonance was saturated during the relaxation delay and the mixing period. Data were zero-filled in the t1 dimension to give a matrix of 2000 × 2000 real points. A sinebell apodization function with a 90° phase shift and a skew factor of 0.7 was used in the t1 and t2 dimensions. Phase-sensitive NOESY experiments in 9:1 H_2O-D_2O were performed using a jump return 1−1 sequence for water suppression as the read pulse (*53*, *54*). Convolution difference was used during processing to minimize the residual water signal (*55*). The NOE mixing time was 250 ms. In the t1 dimension, 512 data points were collected, with 64 scans per FID; the relaxation delay was 1.5 s. In the t2 dimension, 2000 data points were utilized. These experiments were carried out at 10 °C. NMR data were transferred to Indigo workstations (Silicon Graphics, Inc., Mountain View, CA) and processed using FELIX (Molecular Simulations, Inc., San Diego, CA).

Restraints. NOESY spectra at mixing times of 200, 300, and 400 ms were acquired within a single 3-day period. The pulse program was modified with a systematically shifted composite 180° pulse implemented within the mixing period, and composite 90° pulses were used in place of the second and third 90° pulses in the standard pulse sequence (*56*). Footprints were drawn around the cross-peaks for the spectrum measured at a mixing time of 400 ms using FELIX. The same set of footprints was applied to spectra measured at other mixing times. Cross-peak intensities were determined by volume integration of the areas under the footprints.

Classical B-DNA and A-DNA (*57*) were used as reference structures; models were constructed by bonding C10 of BPDE to N[6] of adenine, with the correct stereochemistry and partial charges (*58*). One structure was built from B-DNA with the BP moiety intercalated into the helix; a second was built from A-DNA such that the BP moiety was situated in the major groove of the duplex. These were energy-minimized for 500 iterations by the conjugate gradient method to give the BP-Bi and BP-Ao starting structures used in subsequent calculations. MARDIGRAS (*59*, *60*) was used to iteratively refine the hybrid matrix to optimize the agreement between the calculated and experimental NOE intensities. The NOE intensities were combined as necessary with intensities generated from complete relaxation matrix analysis of a starting DNA structure to generate a hybrid intensity matrix. An isotropic correlation time of 4 ns was used for both sugar and base protons, derived from the τ_c value measured from fluorescence anisotropy (*32*). Calculations using the two DNA starting models generated by INSIGHTII (Molecular Simulations Inc., San Diego, CA), NOE experiments at 3 mixing times, and a τ_c of 4 ns yielded 6 sets of distances. These were pooled; the standard deviations obtained from averaging calculated distances from the 6 sets of data were used as error bounds to provide the NOE restraints used in subsequent rMD calculations.

Restrained Molecular Dynamics. Calculations were performed using X-PLOR (*61*). The force field was derived from CHARMM (*62*) and adapted for restrained MD calculations of nucleic acids. The empirical energy function (*63*) was developed for nucleic acids and treated all hydrogens explicitly. It consisted of energy terms for bonds, bond angles, torsion angles, tetrahedral and planar geometry, hydrogen bonding, and nonbonded interactions including van der Waals and electrostatic forces. The van der Waals energy term was approximated using the Lennard-Jones potential energy function. The electrostatic term used the Coulomb function, based on a full set of partial charges (−1/residue) and a distance-dependent dielectric constant of 4. The nonbonded pair list was updated if any atom moved more than 0.5 Å, and the cutoff radius for nonbonded interactions was 11 Å. All bond lengths involving hydrogens were kept fixed with the SHAKE algorithm (*64*). All calculations were performed in vacuo without explicit counterions. The integration time step was 1 fs.

The effective energy function included terms describing distance and dihedral restraints, which were in the form of square well potentials (*65*). The distance restraints were divided into 4 classes on the basis of the confidence factor obtained from MARDIGRAS. Coupling constants for the sugar protons that displayed well-resolved H1′−H2′ and H1′−H2″ scalar coupling cross-peaks were obtained following simulation using CPANEL, an interactive script that utilized SPHINX and LINSHA (*66*). PSEUROT (*67, 68*) generated the pseudorotational parameters, P and Φ_m, for deoxyribose rings, when resolution permitted. A number of empirical restraints were included. With the exception of the adduct site and immediately adjacent base pairs, the deoxyribose rings were restrained to the C2′-endo conformation. The torsion angles ϵ and ζ were restrained to 155° ± 20° and 254° ± 20°, consistent with B-DNA geometry. This was justified by the observation that there were no unusually shifted ^{31}P resonances in the duplex (*69*), indicating that the backbone geometry was most probably similar to that for B-DNA. Watson−Crick hydrogen-bonding restraints between base pairs were used except at A^6•T^{17} and ^{S,R,S,R}A^7•T^{16}, where experimental evidence for base pairing was not observed.

Sets of rMD calculations were performed using both BP-Bi and BP-Ao starting structures, with A^6 in either the C2′-endo or the C3′-endo conformation. Random velocities fitting a Maxwell−Boltzmann distribution were assigned. Calculations were initiated for 7 ps, with force constants of 10 kcal mol^{-1} A^{-2} for empirical hydrogen bonding and base pair planarity restraints, and 50 kcal mol^{-1} A^{-2} for NOE restraints. The system was then coupled to a heating bath with a target temperature of 900 K for calculations using the BP-Bi starting structure or 1200 K for calculations using the BP-Ao starting structure, which was reached in 3 ps. This temperature was maintained for 17 ps. The molecules were cooled to 300 K over 3 ps and maintained at that temperature for 25 ps of equilibrium dynamics. The force constants for the four classes of NOE restraints were scaled up for 3−5 ps during the heating period to 150, 120, 90, and 60 kcal mol^{-1} A^{-2} in the order of confidence factor. These weights were maintained during the remainder of the heating period and for the first 2 ps of the equilibrium dynamics period and were then scaled down to 50, 40, 30, and 20 kcal mol^{-1} A^{-2} in the order of confidence factor. The dihedral angle and base pair distance force constants were scaled up to 100 kcal mol^{-1} A^{-2} during the same period as for the NOE restraints and scaled back to 20 kcal mol^{-1} A^{-2}, also at the same time as the NOE restraints. Coordinate sets were archived every 0.1 ps, and 40 structures from the last 5 ps were averaged. These average rMD structures were subjected to 300 iterations of conjugate gradient energy minimization to obtain the final structures. Back calculation of theoretical NMR intensities from the emergent structures was performed using CORMA (*70*). The structures were analyzed using DIALS AND WINDOWS 1.0 (*71*).

RESULTS

A combination of UV melting data and a series of ^{1}H spectra obtained at temperatures from 5 to 45 °C indicated that 20 °C was the optimal temperature at which the duplex remained intact and the ^{1}H resonances were the sharpest and best resolved. The SRSR(61,3) adduct destabilized the duplex by a 13 °C reduction in T_m relative to the unmodified duplex.

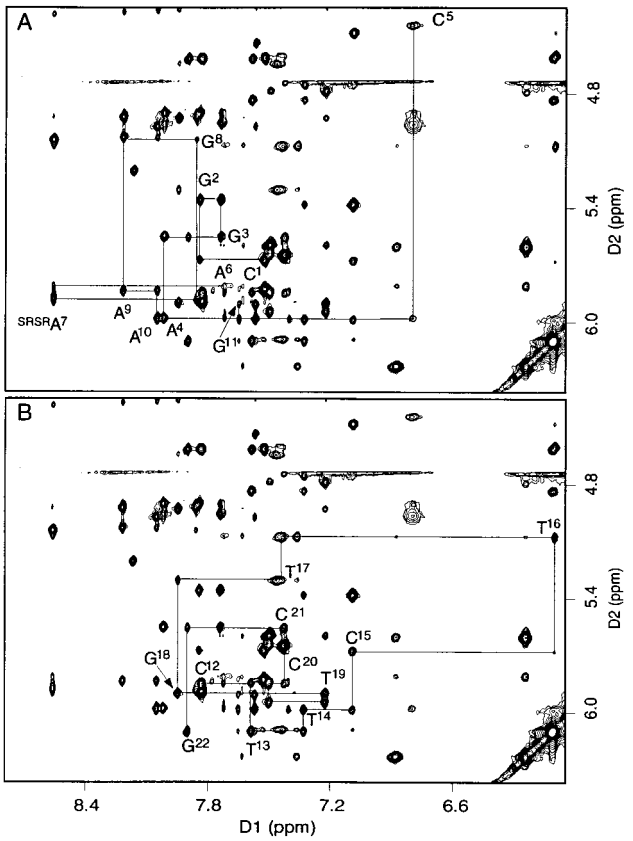

FIGURE 1: A 750 MHz NOESY spectrum at 400 ms mixing time. The aromatic−anomeric region shows the sequential assignment scheme for (A) the modified strand and (B) the complementary strand.

^{1}H Resonance Assignments. (a) Nonexchangeable Protons. Figure 1 shows an expanded NOE spectrum displaying the sequential connectivities (*72, 73*) between the aromatic and anomeric protons of the SRSR(61,3) adduct. For the modified strand, a break in the sequential connectivities was observed between C^5 and A^6. Moreover, weak intranucleotide NOEs were observed between C^5 H6 → C5 H1′ and A^6 H8 → A^6 H1′. The C^5 H5 and H6 and A^6 H8 resonances were broad. A^6 H1′ had a connectivity to ^{SRSR}A^7 H8, but it was weaker than expected for a normal base step, while a normal connectivity was observed from ^{SRSR}A^7 H1′ to G^8 H8. No interruption was observed in the NOE connectivities of the complementary strand. However, broadening of T^{17} H6 was observed along with a weak connectivity between T^{16} H6 and C^{15} H6. The remainder of the bases in both strands appeared to have NOE connectivities characteristic of a B-DNA-like structure.

The assignments of the deoxyribose protons were determined from TOCSY and COSY spectra. Where possible, H5″ resonances were assigned from the observation that for B-DNA the distance between the H5″ proton and the H1′ proton of the 5′ neighboring base was ∼3 Å whereas that between the H5′ proton and the H1′ proton of the 5′ neighboring base was >5 Å. Similarly, for B-DNA the distance between the H5″ proton and the H4′ proton of the 5′-neighboring base was ∼3.4 Å, whereas that between the H5″ proton and H4′ proton of the 5′ neighboring base was

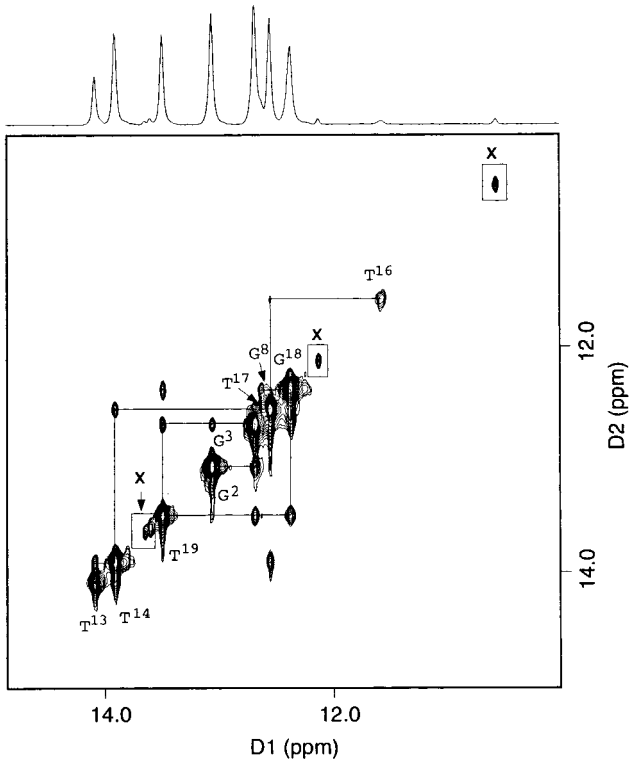

FIGURE 2: A NOESY spectrum at 250 ms mixing time showing sequential connectivities for the imino protons of base pairs G^{2}•$C^{21} \rightarrow A^{10}$•$T^{13}$. The labels represent the imino proton of the designated base. Also shown is a 1D projection of the imino proton resonances. Both 1D and 2D experiments were at 10 °C.

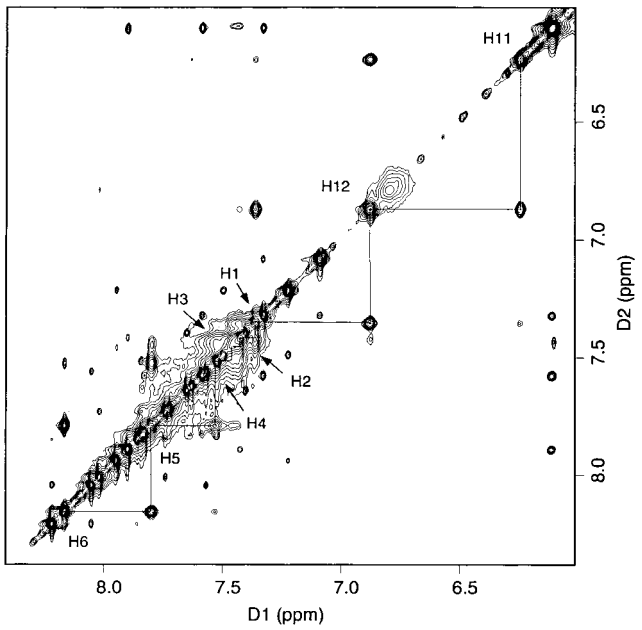

FIGURE 3: An expanded NOESY spectrum of the aromatic−aromatic region at 400 ms mixing time, showing the sequential assignment scheme for the aromatic protons of benzo[a]pyrene. The experiment was at 20 °C.

>5 Å. After the assignment of the H5″ resonances, the H5′ resonances were assigned from the NOESY spectrum at 400 ms mixing time. Nevertheless, in many instances the H5′ and H5″ resonances overlapped, making unambiguous assignments impossible. Table S1 in the Supporting Information lists the chemical shifts of the nonexchangeable protons.

(b) Exchangeable Protons. A total of 8 imino resonances were observed at 10 °C (Figure 2), 6 of which displayed sharp peaks. Sequential assignments (*74*) from base pairs G^{2}•$C^{21} \rightarrow C^{5}$•G^{18} and $^{SRSR}A^{7}$•$T^{16} \rightarrow A^{10}$•$T^{13}$ were obtained unequivocally. The imino resonances of the terminal base pairs were broadened, probably due to increased exchange with solvent. A broad resonance with a cross-peak to G^{18} N1H was observed at 12.5 ppm. This was assigned to T^{17} N3H. Another upfield-shifted and broadened resonance at 11.5 ppm had a weak connectivity to G^{8} N1H. This was assigned to T^{16} N3H. No NOE was observed between T^{16} N3H and T^{17} N3H. Two weak resonances at 13.4 ppm showed strong exchange peaks with H_2O and were tentatively assigned as G^{11} N1H and G^{22} N1H, the terminal nucleotides. Two resonances of low intensity between 11 and 12 ppm were not identified. These did not display exchange peaks with the solvent at temperatures from 5 to 50 °C, which indicated that they were protons that were exchanging very slowly with H_2O. An exchangeable resonance at 6.59 ppm displayed a cross-peak to T^{16} N3H. This resonance was assigned to $^{SRSR}A^{7}$ $N^{6}H_a$. The remainder of the adenine amino protons were not observed due to exchange broadening. The chemical shifts of the exchangeable protons are listed in Table S2 of the Supporting Information.

(c) Benzo[a]pyrene Protons. An expanded region of the NOESY spectrum at 20 °C used for the assignment of pyrenyl protons is shown in Figure 3. The numbering scheme for the benzo[a]pyrene protons is shown in Scheme 1. The 1.9 ppm range of chemical shifts observed was reminiscent of the pyrenyl protons of the SRSR(61,2) adduct in which the BP moiety was found to be intercalated (*32*). The aliphatic ring resonances were assigned from connectivities to benzo[a]pyrene aromatic protons, H6 and H11, and from sequential connectivities between the aliphatic ring protons. A strong NOE was found between benzo[a]pyrene H11 and a resonance at 5.63 ppm. This resonance was assigned to H10. A strong cross-peak was detected between H10 and a resonance at 4.79 ppm. This resonance was assigned to H9. A strong NOE cross-peak was detected between the BP H6 proton and a resonance at 5.21 ppm. This resonance was then assigned to H7. H8 was assigned from a strong cross-peak to H7 and from a weak one to H9. The chemical shifts of the pyrenyl and aliphatic ring resonances are listed in Table S3.

Benzo[a]pyrene-DNA NOEs. A total of 35 NOEs were found; Figure 4 shows a selection of the most resolved of these. Most involved the modified base pair $^{SRSR}A^{7}$•T^{16}, and its 5′ neighbor, A^{6}•T^{17}. The BP H10, H11, and H12 protons, all located on the edge of the adduct closest to the modified adenine, showed intrastrand NOEs to $^{SRSR}A^{7}$ H2. The BP H2, H3, H4, H5, and H6 protons, on the opposite edge of the pyrenyl moiety, showed cross-strand NOEs at the site of adduction to T^{16} CH_3. The BP H1, H2, H3, and H4 protons showed NOEs to T^{16} H6. NOEs were also observed between pyrenyl protons and the deoxyribose of T^{16}. The BP H1, H2, and H3 protons showed NOEs to T^{16} H2′, BP H4 to T^{16} H3′, and BP H1 and H2 to T^{16} H1′. In the 5′ direction, NOEs were observed to the deoxyribose protons of A^{6}. BP H10 showed intrastrand NOEs to A^{6} H2″ and H3′, BP H11 to A^{6} H2′, H2″, H1′, and H3′, and BP H12 to A^{6} H1′ and H3′. Cross-strand NOEs were observed between BP and the base and deoxyribose protons of T^{17}. BP H5 and H6 showed NOEs to T^{17} CH_3, BP H2 and H3 to T^{17}

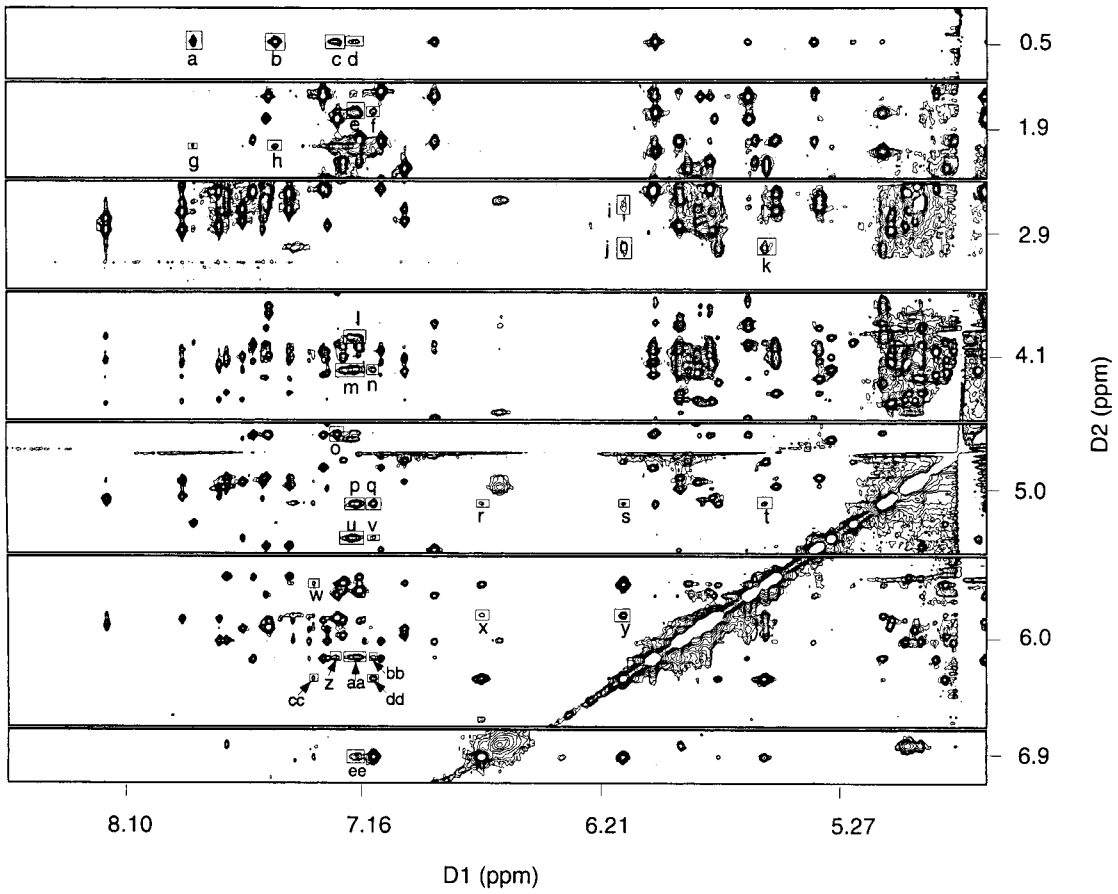

FIGURE 4: Tile plots showing NOE cross-peaks between DNA and benzo[a]pyrene protons. Cross-peaks a−d, $T^{16}CH_3$ → H2−H6; e−f, T^{16} H2′, H2″ → H2, H3 and H1; g−h, T^{17} CH_3 → H5, H6; i−j, A^6 H2′, H2″ → H11; k, A^6 H2 → H10; l−m, T^{17} H5″, H4′ → H2 and H3; n, T^{17} H4′ → H1; o, T^{16} H3′ → H4; p−q, T^{16} H1′ → H2, H1; r, A^6 H1′ → H12; s, A^6 H1′ → H11; t, A^6 H3′ → H10; u, T^{17} H1′ → H2, H3, H11; v, T^{17} H1′ → H1; w, A^7 H2 → H10; x, A^6 H3′ → H12; y, A^6 H3′ → H11; z, T^{16} H6 → H4; aa, bb, T^{16} H6 → H2, H3, and H1; cc, dd, A^7 H2 → H11, H12.

H4′ and H5″, BP H1 to T^{17} H4′, and BP H1, H2, and H3 to T^{17} H1′.

Chemical Shift Perturbations. Adduct-induced chemical shifts were localized to the site of adduction and adjacent base pairs (Figure 5). For the imino protons, a large upfield shift of 2.4 ppm was observed for T^{16} N3H, the imino proton of the adducted base pair. T^{17} N3H, the imino proton of the 5′ neighbor base pair, experienced an upfield shift of 1.1 ppm. For the base protons, chemical shift effects were small, with the exception of the modified base pair, $^{SRSR}A^7$•T^{16}. An upfield chemical shift change of 1.3 ppm was observed for T^{16} H6. Similarly, an upfield chemical shift change of 1.1 ppm was experienced by T^{16} CH_3. The deoxyribose protons exibited chemical shifts localized at the site of adduction, and longer range effects in the 5′ direction, as well. At the site of the adduct, T^{16} H1′ experienced a 0.85 ppm upfield shift. Smaller upfield chemical shifts of 0.35 and 0.5 ppm, respectively, were experienced by T^{16} H2′ and H2″. Longer range upfield chemical shift changes were also observed. C^5 H1′, H2′, and H2″ (two bases to the 5′ direction of the site of lesion) experienced upfield chemical shifts of 0.8−0.9 ppm. C^{15} H2′ and H2″ also experienced upfield chemical shifts of 0.8−0.9 ppm.

NOE Restraints. The MARDIGRAS calculations generated a total of 6 distance sets, each consisting of 595 restraints. After the removal of poor distances that resulted from overlapped NOE intensities or the water presaturation pulse, the 6 sets of distance restraints were averaged, resulting in a total of 532 internuclear distances. Of these distances, 312 were intranucleotide restraints, 185 were interresidue restraints, and 35 were NOEs between the BP and DNA protons. An average of 24 experimental NOE restraints were obtained for each base. The distribution of these restraints for each base is summarized in Table S4 in the Supporting Information. With the exception of A^6 and C^{21}, all bases were restrained by 10 or more intranucleotide NOEs. All bases except for A^4, A^6, and A^9 had 6 or more interbase NOEs. A list of NOE-generated distances along with the upper and lower bounds is shown in Table S5 of the Supporting Information.

Torsion Angle Restraints. Figure 6 shows simulated and experimental COSY cross-peaks for the sugar protons of A^6, as compared to C^{21}. PSEUROT analysis of the simulated spectrum showed that the C2′-endo ↔ C3′-endo equilibrium for the A^6 deoxyribose existed in a 53%−47% ratio, favoring C2′-endo. For the remainder of the deoxyribose rings in this modified oligodeoxynucleotide, the absence of the H2″−H3′ cross-peak in the spectrum indicated that coupling between these two protons was <2 Hz. Therefore the C2′-endo ↔ C3′-endo ratio was in all other instances >84% in favor of C2′-endo. The values for the δ torsional angle, along with the coupling constants (estimated to be acurate to within ±15%) and the line widths used to simulate the

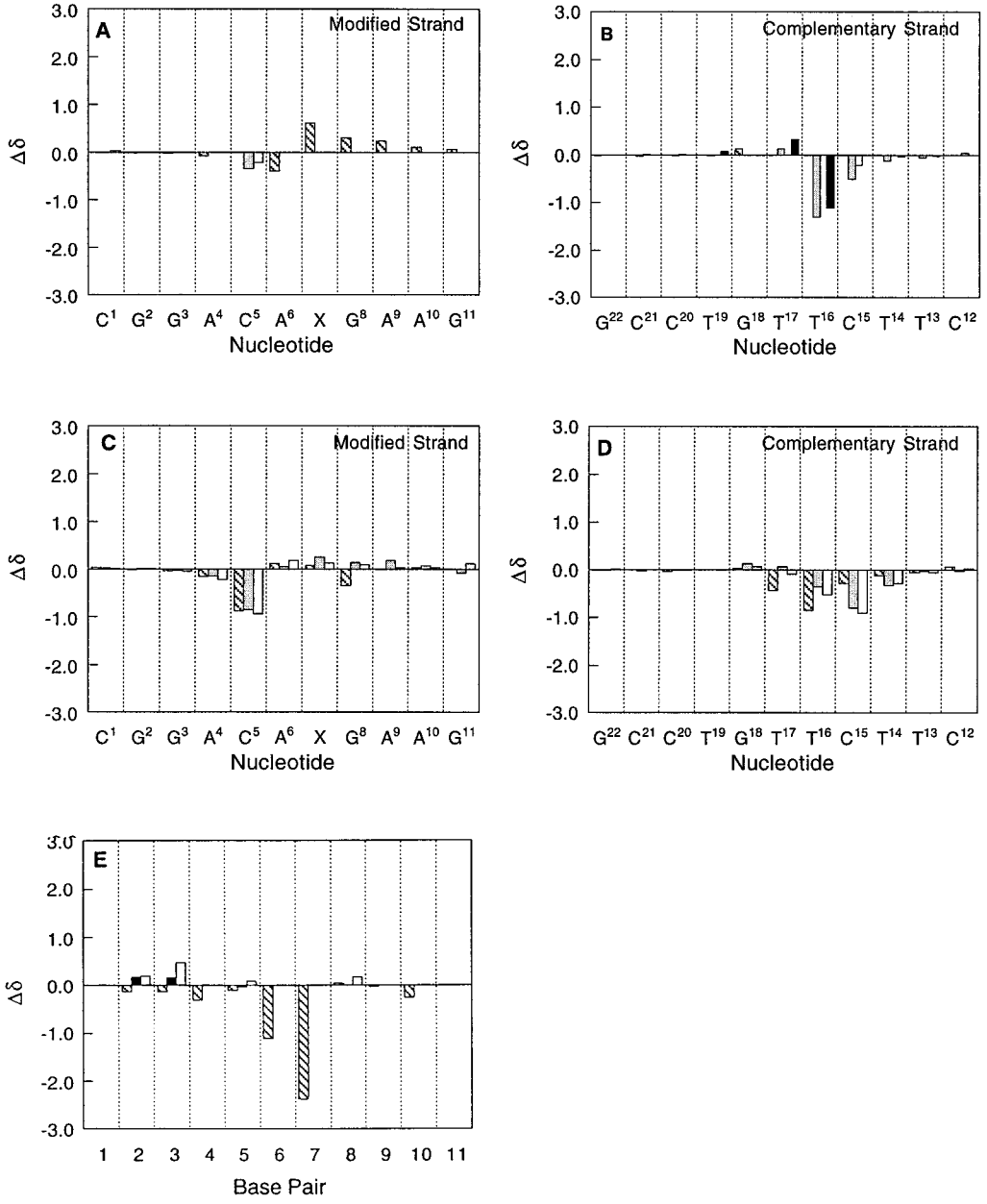

FIGURE 5: Chemical shift changes of selected protons relative to the unmodified *ras61* duplex. (A and B) Major groove protons in the modified and complementary strands, respectively: crosshatched bars, G H8 or A H8; open bars, C H5; solid bars, C H6 and T H6; and dotted bars, T CH_3. (C and D) Minor groove protons in the modified and complementary strands, respectively: crosshatched bars, H1′; dotted bars, H2′; and open bars, H2″, respectively. (E) Exchangeable protons: crosshatched bars, G N1H and T N3H; solid bars, C N4H-(b); and open bars, C N4H(a). Positive $\Delta\delta$ values indicate upfield shifts relative to the *ras61* oligodeoxynucleotide: $\Delta\delta = [\delta_{\text{unmodified oligomer}} - \delta_{\text{modified oligomer}}]$ (ppm).

COSY cross-peaks, are listed in Table S6 in the Supporting Information.

Structural Calculations. Two families of structures were generated from each of the initial structures BP-Bi and BP-Ao. In the first, the sugar ring of A^6 was restrained to C2′-endo geometry, while in the second, it was restrained to C3′-endo geometry. The results of these calculations are shown in Figure 7 which shows an overlay of the 10 structures obtained for each conformation. The structures calculated using the C2′-endo restraints exhibited less overall distortion of the duplex, but resulted in poorer stacking between the intercalated pyrenyl moiety and the 5′ neighbor base pair A^6•T^{17} (Figure 8). The structures calculated using the C3′-endo restraints resulted in greater structural perturbation, manifested by the 1.2 Å calculated displacement toward the major groove for A^6. This resulted in poorer stacking between C^5 and A^6. However, the C3′-endo pucker of the A^6 deoxyribose provided improved stacking between A^6 and the pyrenyl moiety. T^{17}, complementary to A^6, was tilted and extruded toward the major groove for both C2′-endo- and C3′-endo-restrained structures, which probably relieved a steric clash with the pyrenyl moiety. Both sets of calculated structures suggested that BP intercalation resulted in disruptions of H-bonding of the base pairs A^6•T^{17} and $^{SRSR}A^7$•T^{16}.

The precision of the calculated structures was monitored by pairwise calculation of rms deviations (Table 1). The rmsd values between the structures calculated using the 2′-endo and 3′-endo restraints and BP-Ao were 7.20 Å and 7.54 Å, respectively, whereas the corresponding rmsd values when

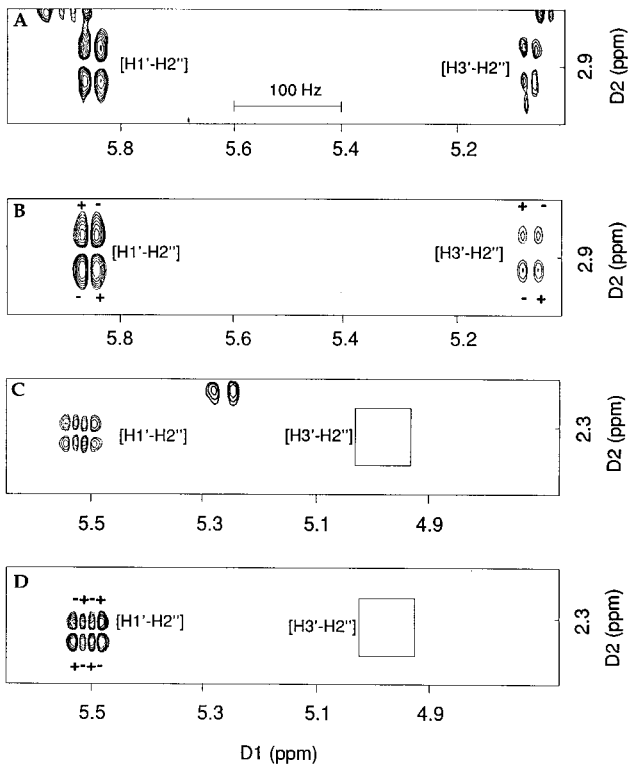

FIGURE 6: Comparison of experimental 2QF−COSY cross-peaks and best-fit simulations of the scalar couplings between H1′ and H2″ and between H3′ and H2″ for A^6 and C^{21}. Panels A and B show the experimental and simulated cross-peaks for the A^6 sugar protons, respectively. Panels C and D show the experimental and simulated cross-peaks for the C^{21} sugar protons, respectively. The best-fit simulation of the A^6 sugar proton scalar couplings was obtained using the coupling constants: H1′−H2′ (5.03 Hz), H1′−H2″ (7.10 Hz), H2′−H3′ (5.80 Hz), H2″−H3′ (5.20 Hz), and H3′−H4′ (5.30 Hz). The best-fit simulations of the C^{21} sugar proton scalar couplings was obtained using the coupling constants: H1′−H2′ (8.50 Hz), H1′−H2″ (6.56 Hz), H2′−H3′ (5.50 Hz), H2″−H3′ (2.50 Hz), and H3′−H4′ (2.08 Hz).

compared with BP-Bi were 2.91 Å and 3.73 Å, respectively. Therefore, the structures calculated using either 2′-endo or 3′-endo restraints were more B-DNA-like. The comparison of the families of structures calculated using either the 2′-endo or 3′-endo retraints revealed that the emergent structures were similar, with the exception of base pairs C^5•G^{18} and A^6•T^{17}, which were differentially restrained. Thus, the overall rmsd between the A^6 C2′-endo- and A^6 C3′-endo-restrained structures was 2.1 Å.

The accuracy of the emergent structures was evaluated with a complete relaxation matrix approach which incorporated the inverse sixth power dependence of the NOE data to determine R_1^x values, using CORMA. The starting structure of neither BP-Ao nor BP-Bi agreed well with the NOE intensities, as revealed by overall R_1^x values obtained for these two structures of 16×10^{-2} and 14×10^{-2}, respectively. The emergent A^6 2′-endo- and A^6 3′-endo-restrained structures showed improved agreement with the data as indicated by lower overall R_1^x values of 7.8×10^{-2} and 8.1×10^{-2}, respectively (Table 1). Despite these improved overall R_1^x values, and consistent with the expectation that the 2′-endo and 3′-endo conformations were in rapid exchange on the NMR time scale, neither the 2′-endo- or the 3′-endo-restrained structures satisfied the NMR data. This was evidenced in the adducted strand by R_1^x values of $20-30 \times 10^{-2}$ for C^5, A^6, and ^{SRSR}A^7 (Figure 9). In contrast, T^{16}, T^{17}, and G^{18}, the nucleotides complementary to C^5, A^6, and ^{SRSR}A^7, exhibited R_1^x values $<10 \times 10^{-2}$, suggesting that the poor fit to the data was limited to the adducted strand at and adjacent to the lesion. In an additional set of calculations, R_1^x values were calculated from the theoretical NOE intensities of a 53%−47% mixture of the emergent structures obtained using the A^6 2′-endo and A^6 3′-endo-restraints. The results are shown in panels E and F of Figure 9. The improved R_1^x values at A^6 and ^{SRSR}A^7 suggested that the fast average blend of deoxyribose conformations at A^6 provided a more reasonable fit to the NOE intensity data. The R_1^x values of C^5 remained high, indicating that, even after taking the rapid conformational averaging at A^6 into account, the structural refinement for this nucleotide remained poor. The inability to satisfactorily refine the duplex structure at C^5 was attributed to an inability to accurately measure distances involving this nucleotide, because of line broadening of the C^5 resonances. This can be observed in Figure 3, in which the broadened C^5 H6 diagonal cross-peak is observed immediately adjacent to the H12 resoance of the BP moiety. The broadening of the C^5 resonances was likely a consequence of the conformational averaging at A^6.

DISCUSSION

The SRSR(61,3) adduct is a sequence isomer of the previously examined SRSR(61,2) adduct, which was located at the first adenine of the *N-ras* codon 61 sequence (*32*). The stereochemistry of adduction for both duplexes was the same; however, the 5′ and 3′ neighboring bases differed. Elucidation of the solution structure of the SRSR(61,3) adduct allowed the role of DNA sequence in modulating benzo[a]pyrene adduct conformation in codon 61 of the *N-ras* gene to be examined. The results of the present work revealed that both the SRSR(61,2) (32) and SRSR(61,3) BP adducts in the *ras61* sequence shared common features. Most notably, both adducts intercalated above the 5′ face of the modified adenine, entering the DNA duplex from the major groove. On the other hand, the NMR data revealed sequence-dependent differences between these two adducts, which may correlate with their biological processing.

Structural Features. The SRSR(61,3) adduct was best described as a mixture of two species in rapid equilibrium on the NMR time scale, one with the C2′-endo conformation at A^6 and the second with the 3′-endo conformation at A^6. Normally, the ensemble of structures which exchange rapidly on the NMR time scale and give rise to the NOEs and J couplings used in the structural refinement process would be assumed to be clustered about a single predominant sugar pucker, C2′-endo for B-type helices. Several approaches have been proposed for modeling the ensemble of deoxyribose pseudorotation states which contribute to NMR data (*75*−*78*). However, in the present instance, DQF−COSY data indicated that the population of sugar pucker states at nucleotide A^6 was not centered on the 2′-endo conformation. Instead, the A^6 deoxyribose was described as an approximately equal ratio of C3′-endo and C2′-endo conformers, in rapid equilibrium. This effectively increased the number of degrees of freedom of the system by a factor of 2, at and adjacent to the lesion site. On the other hand, the adduct-induced perturbation was localized. Therefore, distal to the benzo[a]pyrene lesion, both equilibrating species

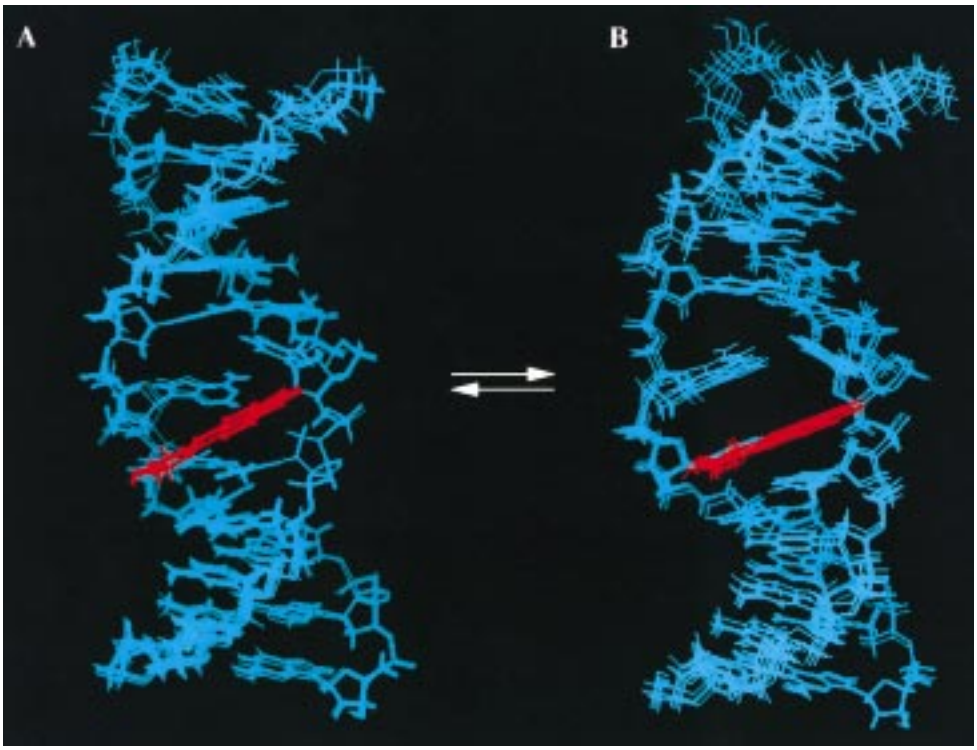

FIGURE 7: Superpositions of the 10 structures obtained from molecular dynamics/simulated annealing for the BP-Ao and BP-Bi initial structures having (A) A^6 in the C2′-endo conformation and (B) A^6 in the C3′-endo conformation.

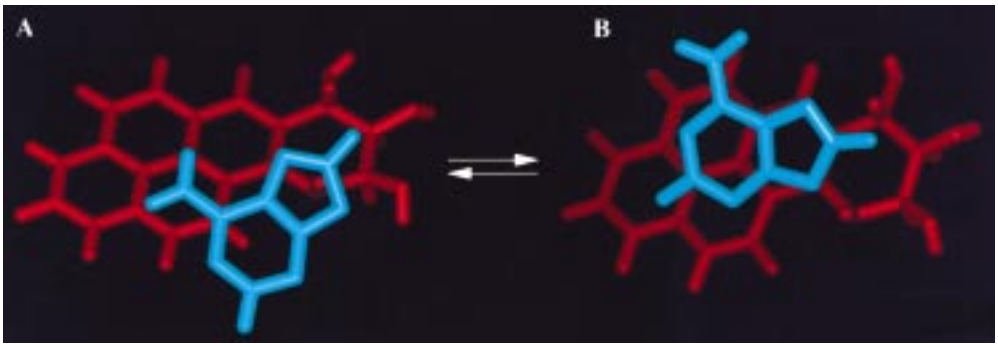

FIGURE 8: Stacking patterns of the BP moiety (colored red) relative to the aromatic rings of A^6 found (A) in the C2′-endo conformation and (B) in the C3′-endo conformation.

exhibited essentially the same structure. To account for this, two families of structures were refined, one of which was restrained to the C2′-endo conformation at A^6, and the other which was restrained to the C3′-endo conformation at A^6. In the absence of these restraints which forced one set of calculations to the C2′-endo conformation at A^6, and the other set to the C3′-endo conformation at A^6, rMD calculations would not have been expected to spontaneously produce these two conformations. Furthermore, as would be predicted by the observation that these equilibrating species were in fast exchange on the NMR time scale, neither the C2′-endo nor the C3′-endo A^6 conformation alone accounted for the experimental NOE intensities.

The emergent structures from the two conformational families differed in that, when the A^6 deoxyribose was in the C3′-endo conformation, A^6 shifted toward the major groove relative to B-DNA. This was consistent with the broadening observed for ^{1}H resonances adjacent to the adducted site in the duplex, including C^5 H5 and H6 and A^6 H8. These were situated above the A^6 purine in the C3′-endo conformer whereas in the C2′-endo conformer they were positioned away from A^6. The major groove shift calculated for base pair A^6 •T^{17} in the C3′-endo structure was consistent with 0.87, 0.84, and 0.93 ppm upfield shifts for C^5 H1′, H2′, and H2″. These were not attributed to ring current shielding from the pyrenyl ring since C^5 H1′, H2′, and H2″ faced the BP aliphatic ring. This was similar to the situation for Z-DNA in which the C3′-endo conformation of the purines shielded the pyrimidine sugar protons (*79*). Since C^5 deoxyribose shifts were ensemble averaged on the NMR time scale, the upfield shift resulting from the C3′-endo conformer may in fact be larger than the observed values. That neither the C2′-endo nor the C3′-endo structure alone could account for the observed NOE data supported the conclusion that this modified oligomer was best described as a mixture of the two conformations, and that the observed NOEs resulted from an average between these two conformations.

In both conformations the BP moiety intercalated from the major groove above the 5′ face of the adducted base pair. This was indicated by NOEs between the BP aromatic protons and both minor and major groove protons of base

Table 1: Analysis of the MD-Generated Structures of the SRSR(61,3) Adduct

NMR Distance Restraints	
total no. of distance restraints	532
inter-residue distance restraints	185
intra-residue distance restraints	312
DNA−BP distance restraints	35
Empirical Restraints	
H-bonding restraints	9
dihedral planarity restraints	11
sugar pucker restraints	22
back-bone torsion angle restraints	40
Structural Statistics	
NMR *R*-factor (R_1^x)[a]	
BP-Ao	0.16
BP-Bi	0.14
A^6 C2′-endo	0.078 ± 0.004
A^6 C3′-endo	0.081 ± 0.010
53%−47% C2′-C3′ mixture	0.075[b]
rmsd of NOE violations (Å)	0.140 ± 0.005
number of NOE violations >0.3 Å in the entire duplex	24 ± 4
root-mean-square deviations from the ideal geometry	
bond length (Å)	0.036 ± 0.002
bond angle (deg)	2.58 ± 0.02
improper angle (deg)	0.72 ± 0.07
pairwise rmsd (Å) over all atoms	
BP-Bi vs C2′-endo	2.91 ± 0.31
BP-Bi vs C3′-endo	3.73 ± 0.38
BP-Ao vs C2′-endo	7.20 ± 0.27
BP-Ao vs C3′-endo	7.54 ± 0.41
C2′-endo vs C2′-endo	0.65 ± 0.33
C3′-endo vs C3′-endo	1.10 ± 0.40
C2′-endo vs C3′-endo	2.10 ± 0.55

[a] Only the inner 9 base pairs were used in the calculations, to exclude end effects. The mixing time was 400 ms. All values for R_1^x are $\times 10^2$. $R_1^x = \sum |(a_o)_i^{1/6} - (a_c)_i^{1/6}| / \sum |(a_o)_i^{1/6}|$, where a_o and a_c are the intensities of observed (non-zero) and calculated NOE crosspeaks. BP-Ao, starting energy-minimized A-DNA with the BP moiety situated in the major groove; BP-Bi, starting energy-minimized B-DNA with the BP moiety intercalated between base pairs 5 and 6; C2′-endo, average of 10 rMD structures starting from BP-Ao and BP−Bi with the sugar moiety of A^6 restrained to C2′-endo conformation; C3′-endo, average of 10 rMD structures starting from BP-Ao and BP-Bi with the sugar moiety of A^6 restrained to C3′-endo conformation. [b] This was calculated by averaging the R_1^x values calculated using a 53%−47% mixture of the theroretical intensity files generated from the potential energy-minimized average structures of the C2′-endo and C3′-endo families, respectively. Note that this represents the overall R_1^x value for the entire duplex. For the comparative R_1^x values at the lesion site, see Figure 9.

pairs A^6•T^{17} and ^{SRSR}A^7•T^{16}. These included BP H2, H3, H4, H5, H6 → T^{16} CH_3, BP H5, H6 → T^{17} CH_3, BP H2 → T^{16} H1′, BP H1, H2 → T^{17} H1′, and BP H10, H11, H12 → A^7 H2. The 1.9 ppm chemical shift distribution of the BP aromatic protons (Figure 3) was consistent with other intercalated PAH adducts (*15, 28, 29, 31*−*34*). Chemical shifts of 1.1 ppm for T^{16} N3H and 2.4 ppm for T^{17} N3H indicated strong ring current shielding consistent with intercalation (Figure 2). Intercalation was also corroborated by minor groove upfield shifts of 0.85, 0.35, and 0.51 ppm for T^{16} H1′, H2′, and H2″, respectively, and upfield shifts of 0.80 and 0.90 ppm, respectively, for C^{15} H2′ and H2″. These would not have been expected if the pyrenyl moiety were in the major groove.

The broadening of T^{16} and T^{17} N3H relative to the other imino proton resonances was attributed both to increased exchange with solvent and to the C2′-endo-C3′-endo conformational exchange of A^6. Intercalation led to a calculated increase in the rise between base pairs A^6•T^{17} and ^{SRRR} A^7•T^{16}. The orientation of the pyrenyl moiety upon the 5′ face of the modified adenine was consistent with the fact that the anticipated NOE between T^{16} N1H and T^{17} N1H was missing (Figure 2). The sharp aliphatic resonances of the benzo[a]pyrene moiety, with weak NOE connectivities between H8 and H10 and H7 and H9, suggested that the C7 and C8 hydroxyls were pseudoaxial, characteristic of the energetically favored (*28, 31, 32*) half-chair conformation.

Sequence Effects. We attribute the conformational differences between the SRSR(61,2) and the SRSR(61,3) adducts to differential stacking patterns between the BP moiety and the DNA bases, a consequence of the sequence difference at the 5′ side of the lesion. In the SRSR(61,2) adduct, the 5′ neighboring base pair is C•G, whereas in the SRSR(61,3) adduct this base pair is A•T. For the SRSR-(61,2) adduct, the pyrenyl moiety stacks with the neighboring purine base, G^{18}, in the complementary strand (*32*), with minor distortion of the duplex. For the SRSR(61,3) adduct, intrastrand BP stacking with the 5′ neighboring purine, A^6, is apparently accommodated by pulling the A^6 deoxyribose into the energetically less favored 3′-endo conformation. We surmise that, in both the SRSR(61,2) and SRSR(61,3) instances, the BP moiety preferably stacks with the 5′ neighboring purine base. For the SRSR(61,3) adduct, this results in a competition between favorable pyrenyl stacking with A^6, which requires the C3′-endo conformation of A^6, versus preservation of the energetically preferred C2′-endo conformation of A^6, which imposes fewer perturbations on the DNA structure. That the NMR spectroscopy was consistent with the existence of a mixture of conformers in rapid equilibrium would suggest that the two conformations are of similar thermodynamic stability.

Biological Significance. A comparison of the two equilibrating conformations for the SRSR(61,3) adduct with the previously examined SRSR(61,2) adduct (*32*) revealed that the solution structure of the SRSR(61,2) adduct and the C2′-endo conformation of the SRSR(61,3) adduct were similar. On the other hand, the C3′-endo conformation of the SRSR-(61,3) adduct differed from the SRSR(61,2) adduct (Figure 10). If these differences are reflected in the biological processing of these adducts, one might predict a common mutagenic outcome for the SRSR(61,2) adduct and the C2′-endo conformation of the SRSR(61,3) adduct, but a different outcome for C3′-endo conformation of the SRSR(61,3) adduct. Emerging results suggest that this may be the case.[4] In one series of experiments with the SRSR(61,3) adduct, polymerization past the adduct by two DNA polymerases was examined in vitro. Polymerases Klenow *exo-* and Sequenase incorporated nucleotides and extended the primer strand differently for the SRSR(61,2) adduct as compared to the SRSR(61,3) adduct. In another series of experiments, the adducted DNA was replicated in vivo, using repair-deficient AB2480 *E. coli* transformed with M13mp7L2 DNA site-specifically modified with the SRSR(61,3) adduct. The SRSR(61,3) adduct induced both A → T transversions and A → G transitions. Previous studies using the SRSR(61,2) adduct yielded A → G mutations exlusively, at a frequency

[4] Irene S. Zegar, Sherry L. Painter, Parvathi Chary, Ritche J. Jabil, Constance M. Harris, Thomas M. Harris, R. Stephen Lloyd, and Michael P. Stone (manuscript in preparation).

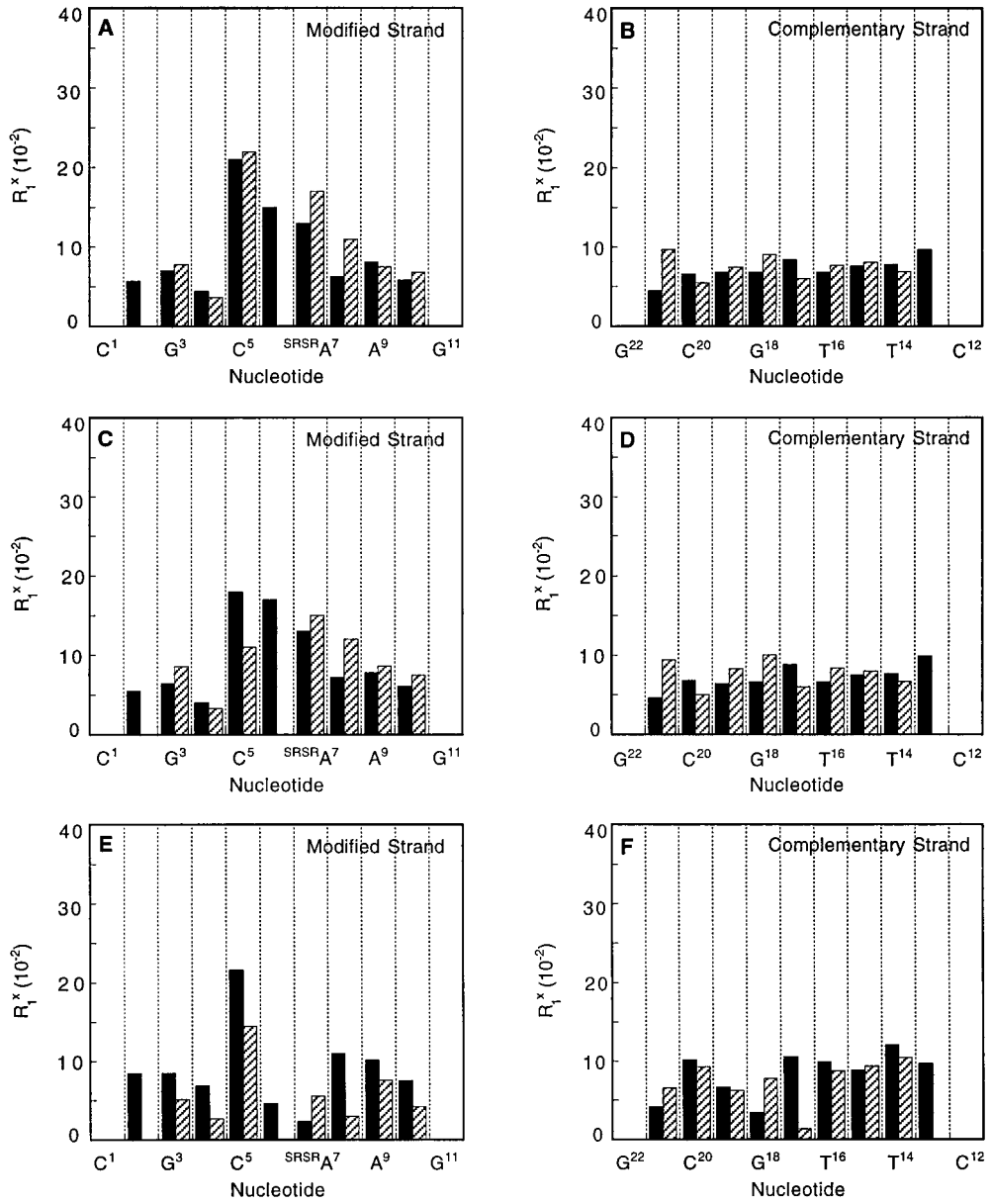

FIGURE 9: A. Bar diagrams showing the per-residue R_1^x values for the modified and complementary strands of the SRSR(61,3) adducts where the solid bars show the intraresidue R_1^x values and the crosshatch bars show the interresidue R_1^x values. Panels A and B show the R_1^x values calculated from the C2′-endo structure. Panels C and D show the R_1^x values calculated from the C3′-endo structure. Panels E and F show the R_1^x values calculated using a 53%−47% mixture of the theoretical intensity files generated from the C2′-endo and the C3′-endo structures, respectively.

of 0.46% (*26*). Thus, initial indications suggest a correlation between the BP SRSR(61,2) (*32*) and SRSR(61,3) adduct conformations and their biological processing. It remains important, however, to emphasize that our understanding of structure−activity relationships for these adducts remains limited. A number of additional factors may play a role in modulating the biological processing of these adducts. Indeed, the exclusivity of A → G mutations at the SRSR-(61,2) site in the *ras61* sequence observed by Chary et al. (*26*) differed from results of Page et al. (*38*), who examined the same adduct, but using a differing bacterial strain. In their experiments, A → T and A → C mutations were generated in addition to A → G mutations.

Comparison with the α-Styrene Oxide Adducts in the ras61 Oligodeoxynucleotide. The adenyl N^6 α-styrene oxide adducts provided precedence for sequence-dependent effects in the *ras61* oligodeoxynucleotide (*44*, *46*). A small sequence effect was observed for the *R*-SO adducts. Although small, it correlated with differences in the processing of the α-SO adducts, as monitored both by site-specific mutagenesis measurements in vivo (*80*) and by polymerase extension experiments in vitro (*81*). Thus, we conclude that modest sequence-dependent conformational differences might well result in measurable differences in adduct processing. A possible explanation is that small sequence-dependent conformational changes might diferentially distort optimal transition-state geometry for DNA replication or repair. Interestingly, a greater sequence effect was observed for the conformation of the *S*-SO adducts (*45*, *46*). Ultimately, it will be of interest to compare the *S*-SO adducts with the BP adducts of corresponding stereochemistry, but unfortunately, it has not been possible to define conditions under which the latter BP adducts yield well-resolved NMR spectra.

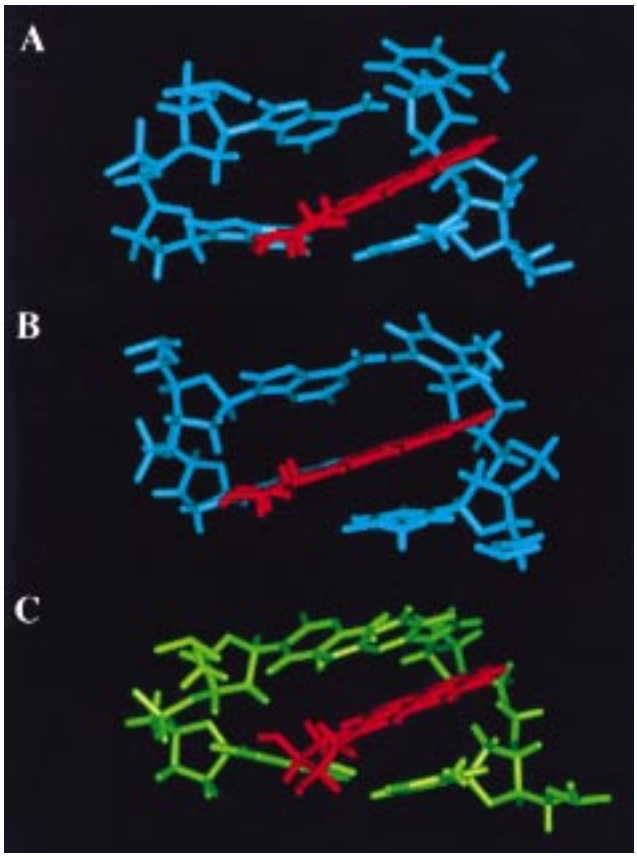

FIGURE 10: Side views from the major groove showing the adducted base pair and its 5′-neighbor for (A) the C2′-endo conformation of the SRSR(61,3) adduct, (B) the C3′-endo conformation for the SRSR(61,3) adduct, and (C) the corresponding structure for the SRSR(61,2) adduct (*32*).

One significant difference between the (−)-(7*S*,8*R*,9*S*,-10*R*)-N^6-[10-(7,8,9,10-tetrahydrobenzo[a]pyrenyl)]-2′-deoxyadenosyl adduct examined opposite T in this study and previously (*32*), and opposite dG (*28*, *29*), the diastereomeric benzo[c]phenanthrene adducts (*33*, *34*), the (−)-7*R*,8*S*,9*R*,10*R*)-N^6-[10-(7,8,9,10-tetrahydrobenzo[a]pyrenyl)]-2′-deoxyadenosyl adduct opposite T (*31*), and the styrene oxide adducts at adenine N^6 (*44*−*46*) was that, in each instance, the PAH adduct intercalated, while the styrene oxide adducts were located in the major groove. This may occur due to greater stacking affinity of the planar polycyclic ring in the PAH compounds. Another contributing factor could be the facile rotation of the styrene oxide adducts about the linkage between the benzylic carbon and the phenyl ring, which is not accessible to the PAH compounds.

Summary. The SRSR(61,3) (−)-(7*S*,8*R*,9*S*,10*R*)-N^6-[10-(7,8,9,10-tetrahydrobenzo[a]pyrenyl)]-2′-deoxyadenosyl adduct was best described as an mixture of two conformations in equilibrium, one in which the A^6 deoxyibose, the 5′ neighbor nucleotide, was in the 3′-endo conformation, and the other in which it was in the 2′-endo conformation. In both instances, the pyrenyl moiety was intercalated on the 5′ face of the adducted adenine, with the pyrenyl moiety inserted into the helix from the major groove. The 3′-endo conformation led to improved stacking between the pyrenyl moiety and the purine ring of A^6. However, greater structural perturbations were induced by the conformation in which A^6 was 3′-endo. The differences observed for these sequence isomers of the ^{SRSR}A BP adduct suggest the importance of understanding adduct structure in the precise sequences such as the *N-ras* codon 61 sequence, in which mutations are directly related to carcinogenesis.

ACKNOWLEDGMENT

Mr. Markus Voehler assisted with NMR spectroscopy and structural refinement. The program CPANEL was generously provided by Dr. Janusz Zdunek, Department of Medical Biochemistry and Biophysics, Umea University, Sweden.

SUPPORTING INFORMATION AVAILABLE

Tables S1, assignments of the nonexchangeable DNA protons, S2, assignments of the exchangeable protons, S3, assignments of the BP protons, S4, the distribution of experimental restraints, S5, the distance restraints, and S6, the deoxyribose J couplings and torsion angles used in the rMD calculations (18 pages). Ordering information is given on any current masthead page.

REFERENCES

1. Guengerich, F. P. (1992) *FASEB J. 6*, 745−748.
2. Sims, P., Grover, P. L., Swaisland, A., Pal, K., and Hewer, A. (1974) *Nature 252*, 326−327.
3. Yagi, H., Hernandez, O., and Jerina, D. M. (1975) *J. Am. Chem. Soc. 97*, 6681−6683.
4. Beland, F. A., and Harvey, R. G. (1976) *J. Chem. Soc., Chem. Commun.* 84−85.
5. Weinstein, I. B., Jeffrey, A. M., Jennette, K. W., and Blobstein, S. H. (1976) *Science 193*, 592−595.
6. King, H. W. S., Osborne, M. R., Beland, F. A., Harvey, R. G., and Brookes, P. (1976) *Proc. Natl. Acad. Sci. U.S.A. 73*, 2679−2681.
7. Jeffrey, A. M., Weinstein, I. B., Jennette, K. W., Grzeskowiak, K., Nakanishi, K., Harvey, R. G., Autrup, H., and Harris, C. (1977) *Nature 269*, 348−350.
8. Nakanishi, K., Kasai, H., Cho, H., Harvey, R. G., Jeffery, A. M., Jennette, K. W., and Weinstein, I. B. (1977) *J. Am. Chem. Soc. 99*, 258−260.
9. Newbold, R. F., and Brookes, P. (1976) *Nature 261*, 52−54.
10. Huberman, E., Sachs, L., Yang, S. K., and Gelboin, H. V. (1976) *Proc. Natl. Acad. Sci. U.S.A. 73*, 607−611.
11. Cosman, M., De Los Santos, C., Fiala, R., Hingerty, B. E., Singh, S. B., Ibanez, V., Margulis, L. A., Live, D., Geacintov, N. E., Broyde, S., and Patel, D. J. (1992) *Proc. Natl. Acad. Sci. U.S.A. 89*, 1914−1918.
12. De Los Santos, C., Cosman, M., Hingerty, B. E., Ibanez, V., Margulis, L. A., Geacintov, N. E., Broyde, S., and Patel, D. J. (1992) *Biochemistry 31*, 5245−5252.
13. Cosman, M., De Los Santos, C., Fiala, R., Hingerty, B. E., Ibanez, V., Luna, E., Harvey, R., Geacintov, N. E., Broyde, S., and Patel, D. J. (1993) *Biochemistry 32*, 4145−4155.
14. Cosman, M., Fiala, R., Hingerty, B. E., Amin, S., Geacintov, N. E., Broyde, S., and Patel, D. J. (1994) *Biochemistry 33*, 11518−11527.
15. Cosman, M., Fiala, R., Hingerty, B. E., Amin, S., Geacintov, N. E., Broyde, S., and Patel, D. J. (1994) *Biochemistry 33*, 11507−11517.
16. Fountain, M. A., and Krugh, T. R. (1995) *Biochemistry 34*, 3152−3161.
17. Feng, B., Gorin, A., Hingerty, B. E., Geacintov, N. E., Broyde, S., and Patel, D. J. (1997) *Biochemistry 36*, 13769−13779.
18. Cosman, M., Xu, R., Hingerty, B. E., Amin, S., Harvey, R. G., Geacintov, N. E., Broyde, S., and Patel, D. J. (1995) *Biochemistry 34*, 6247−6260.
19. Zegar, I. S., Setayesh, F. R., DeCorte, B. L., Harris, C. M., Harris, T. M., and Stone, M. P. (1996) *Biochemistry 35*, 4334−4348.

20. Setayesh, F. R., DeCorte, B. L., Horton, P., Harris, C. M., Harris, T. M., and Stone, M. P. (1998) *Chem. Res. Toxicol. 11*, 766−777.
21. Jennette, K. W., Jeffery, A. M., Blobstein, S. H., Beland, F. A., Harvey, R. G., and Weinstein, I. B. (1977) *Biochemistry 16*, 932−938.
22. Osborne, M. R., Jacobs, S., Harvey, R. G., and Brookes, P. (1981) *Carcinogenesis 2*, 553−558.
23. Wei, S. J., Chang, R. L., Wong, C. Q., Bhachech, N., Cui, X. X., Hennig, E., Yagi, H., Sayer, J. M., Jerina, D. M., Preston, B. D., and Conney, A. H. (1991) *Proc. Natl. Acad. Sci. U.S.A. 88*, 11227−11230.
24. Wei, S. J., Chang, R. L., Bhachech, N., Cui, X. X., Merkler, K. A., Wong, C. Q., Hennig, E., Yagi, H., Jerina, D. M., and Conney, A. H. (1993) *Cancer Res. 53*, 3294−3301.
25. Wei, S. J., Chang, R. L., Hennig, E., Cui, X. X., Merkler, K. A., Wong, C. Q., Yagi, H., Jerina, D. M., and Conney, A. H. (1994) *Carcinogenesis 15*, 1729−1735.
26. Chary, P., Latham, G. J., Robberson, D. L., Kim, S. J., Han, S., Harris, C. M., Harris, T. M., and Lloyd, R. S. (1995) *J. Biol. Chem. 270*, 4990−5000.
27. Chary, P., and Lloyd, R. S. (1995) *Nucleic Acids Res. 23*, 1398−1405.
28. Schurter, E. J., Yeh, H. J. C., Sayer, J. M., Lakshman, M. K., Yagi, H., Jerina, D. M., and Gorenstein, D. G. (1995) *Biochemistry 34*, 1364−1375.
29. Yeh, H. J. C., Sayer, J. M., Liu, X., Altieri, A. S., Byrd, R. A., Lakshman, M. K., Yagi, H., Schurter, E. J., Gorenstein, D. G., and Jerina, D. M. (1995) *Biochemistry 34*, 13570−13581.
30. Schwartz, J. L., Rice, J. S., Luxon, B. A., Sayer, J. M., Xie, G., Yeh, H. J., Liu, X., Jerina, D. M., and Gorenstein, D. G. (1997) *Biochemistry 36*, 11069−11076.
31. Schurter, E. J., Sayer, J. M., Oh-hara, T., Yeh, H. J. C., Yagi, H., Luxon, B. A., Jerina, D. M., and Gorenstein, D. G. (1995) *Biochemistry 34*, 9009−9020.
32. Zegar, I. S., Kim, S. J., Johansen, T. N., Horton, P., Harris, C. M., Harris, T. M., and Stone, M. P. (1996) *Biochemistry 35*, 6212−6224.
33. Cosman, M., Fiala, R., Hingerty, B. E., Laryea, A., Lee, H., Harvey, R. G., Amin, S., Geacintov, N. E., Broyde, S., and Patel, D. (1993) *Biochemistry 32*, 2488−2497.
34. Cosman, M., Laryea, A., Fiala, R., Hingerty, B. E., Amin, S., Geacintov, N. E., Broyde, S., and Patel, D. J. (1995) *Biochemistry 34*, 1295−1307.
35. Mackay, W., Benasutti, M., Drouin, E., and Loechler, E. L. (1992) *Carcinogenesis 13*, 1415−1425.
36. Shukla, R., Liu, T., Geacintov, N. E., and Loechler, E. L. (1997) *Biochemistry 36*, 10256−10261.
37. Jelinsky, S. A., Liu, T., Geacintov, N. E., and Loechler, E. L. (1995) *Biochemistry 34*, 13545−13553.
38. Page, J. E., Zajc, B., Oh-hara, T., Lakshman, M. K., Sayer, J. M., Jerina, D. M., and Dipple, A. (1998) *Biochemistry 37*, 9127−9137.
39. Geacintov, N. E., Cosman, M., Hingerty, B. E., Amin, S., Broyde, S., and Patel, D. J. (1997) *Chem. Res. Toxicol. 10*, 111−146.
40. Suh, M., Jankowiak, R., Ariese, F., Mao, B., Geacintov, N. E., and Small, G. J. (1994) *Carcinogenesis 15*, 2891−2898.
41. Xu, R., Mao, B., Amin, S., and Geacintov, N. (1998) *Biochemistry 37*, 769−778.
42. Barbacid, M. (1987) *Annu. Rev. Biochem. 56*, 779−827.
43. Feng, B., and Stone, M. P. (1995) *Chem. Res. Toxicol. 8*, 821−832.
44. Feng, B., Zhou, L., Passarelli, M., Harris, C. M., Harris, T. M., and Stone, M. P. (1995) *Biochemistry 34*, 14021−14036.
45. Feng, B., Voehler, M. W., Zhou, L., Passarelli, M., Harris, C. M., Harris, T. M., and Stone, M. P. (1996) *Biochemistry 35*, 7316−7329.
46. Stone, M. P., and Feng, B. (1996) *Magn. Reson. Chem. 34*, S105−S114.
47. Schmitz, U., and James, T. L. (1995) *Methods Enzymol. 261*, 3−44.
48. Kim, S. J., Stone, M. P., Harris, C. M., and Harris, T. M. (1992) *J. Am. Chem. Soc. 114*, 5480−5481.
49. Kim, S. J., Harris, C. M., Koreeda, M., and Harris, T. M. (1991) *Tetrahedron Lett. 32*, 6073−6076.
50. Harris, T. M., Harris, C. M., Kim, S. J., Kim, H. Y., and Zhou, L. (1994) in *Polycyclic Aromatic Compounds* (Cavalieri, E., and Rogan, E., Eds.) pp 9−16, Harwood Academic Press, Philadelphia, PA.
51. Borer, P. N. (1975) *Handbook of biochemistry and molecular biology*, CRC Press, Cleveland.
52. Pulkrabek, P., Leffler, S., Weinstein, I. B., and Grunberger, D. (1977) *Biochemistry 16*, 3127−3132.
53. Bax, A., Sklenar, V., Clore, G. M., and Gronenborn, A. M. (1987) *J. Am. Chem. Soc. 109*, 6511−6513.
54. Sklenar, V., Brooks, B. R., Zon, G., and Bax, A. (1987) *FEBS Lett. 216*, 249−252.
55. Marion, D., Ikura, M., and Bax, A. (1989) *J. Magn. Reson. 84*, 425−430.
56. Bodenhausen, G., Kogler, H., and Ernst, R. R. (1984) *J. Magn. Reson. 58*, 370−388.
57. Arnott, S., and Hukins, D. W. L. (1972) *Biochem. Biophys. Res. Commun. 47*, 1504−1509.
58. Hingerty, B. E., Figueroa, S., Hayden, T. L., and Broyde, S. (1989) *Biopolymers 28*, 1195−1222.
59. Borgias, B. A., and James, T. L. (1990) *J. Magn. Reson. 87*, 475−487.
60. Liu, H., Tonelli, M., and James, T. L. (1996) *J. Magn. Reson. Ser. B 111*, 85−89.
61. Brunger, A. T. (1992) in *X-Plor. Version 3.1. A system for X-ray Crystallography and NMR*, Yale University Press, New Haven, CT.
62. Brooks, B. R., Bruccoleri, R. E., Olafson, B. D., States, D. J., Swaminathan, S., and Karplus, M. (1983) *J. Comput. Chem. 4*, 187−217.
63. Nilsson, L., Clore, G. M., Gronenborn, A. M., Brunger, A. T., and Karplus, M. (1986) *J. Mol. Biol. 188*, 455−475.
64. Ryckaert, J.-P., Ciccotti, G., and Berendsen, H. J. C. (1977) *J. Comput. Phys. 23*, 327−341.
65. Clore, G. M., Gronenborn, A. M., Carlson, G., and Meyer, E. F. (1986) *J. Mol. Biol. 190*, 259−267.
66. Widmer, H., and Wuthrich, K. (1986) *J. Magn. Reson. 70*, 270−279.
67. De Leeuw, F. A. A. M., and Altona, C. (1983) *J. Comput. Chem. 4*, 428−437.
68. De Leeuw, F. A. A. M., and Altona, C. (1983) *Quant. Chem. Prog. Bull. 3*, 69.
69. Gorenstein, D. G. (1992) *Methods Enzymol. 211*, 254−286.
70. Keepers, J. W., and James, T. L. (1984) *J. Magn. Reson. 57*, 404−426.
71. Ravishankar, G., Swaminathan, S., Beveridge, D. L., Lavery, R., and Sklenar, H. (1989) *J. Biomol. Struct. Dyn. 6*, 669−699.
72. Reid, B. R. (1987) *Q. Rev. Biophys. 20*, 2−28.
73. Patel, D. J., Shapiro, L., and Hare, D. (1987) *Q. Rev. Biophys. 20*, 35−112.
74. Boelens, R., Scheek, R. M., Dijkstra, K., and Kaptein, R. (1985) *J. Magn. Reson. 62*, 378−386.
75. Schmitz, U., Ulyanov, N. B., Kumar, A., and James, T. L. (1993) *J. Mol. Biol. 234*, 373−389.
76. Ulyanov, N. B., Schmitz, U., and James, T. L. (1993) *J. Biomol. NMR 3*, 547−568.
77. James, T. L. (1994) *Methods Enzymol. 239*, 416−439.
78. Ulyanov, N. B., and James, T. L. (1995) *Methods Enzymol 261*, 90−120.
79. Giessner-Prettre, C., Pullman, B., Tran-Dinh, S., Neumann, J. M., Huynh-Dinh, T., and Igolen, J. (1984) *Nucleic Acids Res. 12*, 3271−3281.
80. Latham, G. J., Zhou, L., Harris, C. M., Harris, T. M., and Lloyd, R. S. (1993) *J. Biol. Chem. 268*, 23427−23434.
81. Latham, G. J., Harris, C. M., Harris, T. M., and Lloyd, R. S. (1995) *Chem. Res. Toxicol. 8*, 422−430.

BI9817616